APPLIED GEOPHYSICS, Vol.12, No.2 (June 2015), P. 169-178, 11 Figures.
DOI: 10.1007/s11770-015-0485-1

A fast-convergence POCS seismic denoising and reconstruction method*

Ge Zi-Jian[1,2], Li Jing-Ye♦[1,2], Pan Shu-Lin[3], and Chen Xiao-Hong[1,2]

Abstract: The efficiency, precision, and denoising capabilities of reconstruction algorithms are critical to seismic data processing. Based on the Fourier-domain projection onto convex sets (POCS) algorithm, we propose an inversely proportional threshold model that defines the optimum threshold, in which the descent rate is larger than in the exponential threshold in the large-coefficient section and slower than in the exponential threshold in the small-coefficient section. Thus, the computation efficiency of the POCS seismic reconstruction greatly improves without affecting the reconstructed precision of weak reflections. To improve the flexibility of the inversely proportional threshold, we obtain the optimal threshold by using an adjustable dependent variable in the denominator of the inversely proportional threshold model. For random noise attenuation by completing the missing traces in seismic data reconstruction, we present a weighted reinsertion strategy based on the data-driven model that can be obtained by using the percentage of the data-driven threshold in each iteration in the threshold section. We apply the proposed POCS reconstruction method to 3D synthetic and field data. The results suggest that the inversely proportional threshold model improves the computational efficiency and precision compared with the traditional threshold models; furthermore, the proposed reinserting weight strategy increases the SNR of the reconstructed data.

Keywords: POCS, Fourier transform, threshold model, reconstruction, denoising

Introduction

Undersampling and missing data are common problems in field data acquisition. Irregularly missing data strongly affect processing methods such as time-lapse seismic repeatability processing, surface-related multiple elimination (SRME), and prestack migration. Therefore, regularization needs to be applied to irregularly missing data.

Seismic data regularization can be divided into two categories. The first category comprises methods based on signal processing principles. The second category consists of wave-equation-based methods (Ronen, 1987; Malcolmet et al., 2005) that reconstruct the seismic volume by using subsurface velocity data.

Manuscript received by the Editor February 7, 2015; revised manuscript received May 10, 2015.
*The research work is supported by the National Natural Science Foundation of China (Nos. U1262207 and 41204101) and the National Science and Technology Major Project of China (No. 2011ZX05019-006).
1. State Key Laboratory of Petroleum Resources and Prospecting, China University of Petroleum, Beijing 102249, China.
2. CNPC Key Laboratory of Geophysical Prospecting, China University of Petroleum, Beijing 102249, China.
3. School of Geoscience and Technology, Southwest Petroleum University, Chengdu 610500, China.
♦Corresponding author: Li Jing-Ye (Email: ljy3605@sina.com)

Within the first category, one group of methods relies on transforms, such as the Fourier transform (Duijndamet et al., 1999; Trad, 2009), the Radon transform (Kabir and Verschuur, 1995; Trad et al., 2002), and the curvelet transform (Naghizadeh and Sacchi, 2010; Liu et al., 2011; Kong et al., 2012). Another group of methods relies on prediction-error filtering techniques (Spitz, 1991; Naghizadeh and Sacchi, 2009). These methods use the predictability of linear events in the frequency–space domain to interpolate aliased data at high frequencies with filters derived from low frequencies. Finally, a third group of methods is based on rank reduction (Trickett et al, 2010; Kreimer and Sacchi, 2011). Properly sampled multichannel data are embedded into a low-rank Hankel matrix. Because noise and missing data increase the rank of the Hankel matrix, rank reduction methods are used to attenuate noise and recover missing traces.

The reconstruction method known as projection onto convex sets (POCS) is based on the Gerchberg –Saxton iterative algorithm (Gerchberg and Saxton, 1972; Li and Du, 2003) and is widely used in signal and image reconstruction. Papoulis (1975) used the POCS reconstruction method to recover a band-limited signal from a given subsegment of the signal. Menke (1991) applied the POCS method to interpolate topography and well log data. Abma and Kabir (2006) used the POCS method to interpolate missing seismic observations. They pointed out that the threshold is the key parameter in POCS reconstruction, and used a linear threshold in the iterations. Galloway and Sacchi (2007) and Gao et al. (2010) used an exponential threshold to improve the convergence of the POCS reconstruction method. Wang et al. (2010) used graphics processing units (GPU) to accelerate the POCS interpolation. Oropeza and Sacchi (2011) presented a rank reduction algorithm for the simultaneous reconstruction and random noise attenuation of seismic data, and used a linear descending weight coefficient with increasing number of iterations to increase the SNR of the reconstructed data. Gao et al. (2013) presented a data-driven threshold to improve the convergence of the POCS algorithm. In addition, a constant reinserting weight was used to minimize the effect of noise in the final reconstruction of the seismic volume. Zhang and Chen (2013) used the exponential threshold model $e^{-\sqrt{x}}\ (0 \le x \le 1)$ in the curvelet domain, which show faster convergence and higher precision compared with traditional exponential threshold. Wang and Zhang (2014) analyzed the effect of the interval between two neighboring threshold on convergence and developed a new exponential threshold to further speed the convergence of POCS reconstruction algorithm.

Presently, the size of wide-azimuth and high-density data limits the computational efficiency and precision of seismic reconstruction algorithms. In the case of the POCS seismic reconstruction algorithm, evaluation criteria for the optimum threshold have not been defined; furthermore, previous threshold models and weighted reinsertion strategies do not account for the different features of the seismic data, which minimizes computational efficiency, calculation precision, and reconstruction flexibility. Based on previous work, we present the inversely proportional threshold model and add a dependent variable to the denominator of the inversely proportional threshold model to improve the computational efficiency, calculation precision, and flexibility of the reconstruction algorithm. The weighted reinsertion strategy and the data-driven model increase the signal-to-noise (SNR) of the reconstructed seismic data.

Theory and methodology

Projection onto convex sets reconstruction in the frequency-space domain

Gao et al. (2010) transformed the POCS reconstruction method from the time-domain to the frequency-domain and then applied thresholds to every frequency component in the iteration process to eliminate the noncoherent noise, successfully recovering the missing traces. In the time-domain method, a forward and inverse Fourier transform are performed at each iteration. However, we only need to apply the forward Fourier transform as a function of time before the first iteration and the inverse Fourier transform after the last iteration. Thus, the modified method cuts the computational cost by about 30% for 3D seismic data. Each iteration in the frequency-domain method comprises five steps: (1) perform the 2D forward Fourier transform for every frequency component $\mathbf{D}(f, x, y)$ to obtain f–k_x–k_y-domain data; (2) apply a threshold to the transformed data and remove the spectral components that are smaller than the threshold; (3) perform an inverse 2D Fourier transform to the modified data; (4) reinsert the original f–x–y-domain traces into the inversely transformed data; and (5) repeat steps 1 to 4 until the deviation between the reconstructed and original data satisfies the termination condition.

For irregularly missing 3D seismic data $\mathbf{D}(f, x, y)$, the POCS reconstruction method can be expressed as (Oropeza and Sacchi, 2011)

$$\mathbf{D}_k\left(f,x,y\right)=\mathbf{D}\left(f,x,y\right)+\left[\mathbf{I}-\mathbf{S}\left(x,y\right)\right]\mathbf{F}_{x,y}{}^{-1}\mathbf{T}_k\mathbf{F}_{x,y}\mathbf{D}_{k-1},$$
$$k=1,2,...,N, \quad (1)$$

where k is the k^{th} iteration, f is the frequency, $\mathbf{D}_k$ denotes the reconstructed f–x–y-domain data at iteration k, $\mathbf{I}$ is the unit matrix, $\mathbf{F}_{x,y}$ and $\mathbf{F}_{x,y}{}^{-1}$ denote the 2D forward and inverse Fourier transform, respectively, for space variables x and y, and $\mathbf{S}(x, y)$ represents the sampling operator, where $\mathbf{S}(x, y) = 1$ for the observed traces and $\mathbf{S}(x, y) = 0$ for the missing traces.

At each iteration, we need to apply a threshold to the transformed data. The threshold operator $\mathbf{T}_k$ is

$$\mathbf{T}_k\left(f,k_x,k_y\right)=\begin{cases}1, & \left|\mathbf{D}_k\left(f,k_x,k_y\right)\right|\ge p_k\\ 0, & \left|\mathbf{D}_k\left(f,k_x,k_y\right)\right|< p_k\end{cases}, \quad p_k\in\mathbf{P}, \quad (2)$$

where k_x and k_y are the wavenumbers for space variables x and y, $\mathbf{P}$ represents the N-dimensional threshold set, $\mathbf{P} = \{p_1, p_2, \ldots, p_N\}$ satisfies $p_1 > p_2 > \ldots > p_N$, and N denotes the maximum number of iterations.

The inversely proportional threshold model

Abma and Kadir (2006) pointed out that strong events are well interpolated using few iterations, whereas weak events require significantly more iterations. Because small and large coefficients correspond to weak and strong events, the evaluation criteria for the optimum threshold, when the threshold model simulates a real spectrum energy, are the following. The larger the descent rate of the threshold in the large-coefficient section is, the faster the convergence is, whereas the smaller the descent rate of the threshold in the small-coefficient section is, the higher the calculation precision is.

The existing threshold model is limited in its adaptability because of the difference of the distribution of the data spectrum. The construction of an optimum threshold model for seismic data will improve the interpolation efficiency in large datasets and will minimize costs. Considering the inversely proportional model ($y = 1/x$, $x \neq 0$) with larger descent rate than the exponential model in the large-coefficient section, we propose an inversely proportional threshold model to satisfy the evaluation criteria. The new threshold is

$$p_k^{\text{inv}}=\frac{a}{k}+b, \quad k=1,2,...,N. \quad (3)$$

For $k = 1$, $p_1^{\text{inv}} = p_{\max}$, and for $k = N$, $p_N^{\text{inv}} = p_{\min}$. $p_{\max}$ and $p_{\min}$ correspond to the maximum and minimum spectrum energy components

$$p_{\max}=a+b, \quad (4)$$

$$p_{\min}=\frac{a}{N}+b, \quad (5)$$

$$a=\frac{N\left(p_{\max}-p_{\min}\right)}{N-1} \text{ and } b=\frac{Np_{\min}-p_{\max}}{N-1}$$

can be obtained from equations (4) and (5). Once the maximum number of iterations is set, equation (3) is difficult to fit seismic data with variable spectrum energy distribution. To improve the flexibility of the proposed threshold, we obtain the inversely proportional model with arbitrary descent rate by adjusting the dependent variable q added to the denominator of equation (3). Hence, equation (3) changes to

$$p_k^{\text{inv}}=\frac{a}{k^q}+b, \quad k=1,2,...,N. \quad (6)$$

Similarly, we obtain

$$a=\frac{N^q\left(p_{\max}-p_{\min}\right)}{N^q-1} \text{ and } b=\frac{N^q p_{\min}-p_{\max}}{N^q-1},$$

where q is an arbitrary real number larger than zero and in most cases $1 \le q \le 3$.

Descending weight coefficient and the data-driven model

To account for the deficiency of the standard POCS interpolation in denoising, Oropeza and Sacchi (2011) used a weighted reinsertion strategy for noisy traces. Then, the algorithm described by equation (1) transforms to

$$\mathbf{D}_k\left(f,x,y\right)$$
$$=Q\mathbf{D}\left(f,x,y\right)+\left[\mathbf{I}-Q\mathbf{S}\left(x,y\right)\right]\mathbf{F}_{x,y}{}^{-1}\mathbf{T}_k\mathbf{F}_{x,y}\mathbf{D}_{k-1}, \quad (7)$$
$$k=1,2,...,N,$$

where Q is the weight coefficient, $0 \le Q \le 1$. For $Q = 1$, we obtain the standard POCS reconstruction using equation (1) and inserting the observed data in the reconstructed data.

In POCS reconstruction algorithm, the thresholds in the early iterations are used to preserve the strong events; thus, most of the observed data are reinserted in the reconstructed data for the efficient recovery of strong events. The smaller thresholds in the final iterations are good for recovering weak events strongly affected by noise; thus, decreasing weight coefficient Q is good for

noise attenuation and the reconstruction of weak events. Based on the analysis above and given the variability of the spectrum energy, the proposed weighing strategy in the data-driven model bases on data itself to flexibly calculate the reinserting weight and is expressed as

$$Q_k = \frac{p_k^{\mathrm{dri}}\left(Q_{\max} - Q_{\min}\right)}{p_{\max} - p_{\min}}, \quad k = 1, 2, ..., N, \tag{8}$$

where Q_k denotes the new threshold at iteration k, p_k^{dri} denotes the data-driven threshold (Gao et al., 2013), $p_{\max}$ and $p_{\min}$ correspond to the maximum and minimum threshold, and $Q_{\max}$ and $Q_{\min}$ are respectively the maximum ($Q_{\max} = 1$) and minimum weight ($Q_{\min} = 0$).

The reconstructed evaluation parameter definition

The reconstructed evaluation parameter is an important index for the quality of the reconstruction and is defined as (Hennenfent and Herrmann, 2006)

$$E_{\mathrm{mode}} = 20\log_{10}\left(\frac{\left\|\mathbf{D}^{\mathrm{ori}}(f,x,y)\right\|_2}{\left\|\mathbf{D}^{\mathrm{ori}}(f,x,y) - \mathbf{D}^{\mathrm{rec}}(f,x,y)\right\|_2}\right), \tag{9}$$

where $\mathbf{D}^{\mathrm{ori}}(f, x, y)$ is the complete seismic dataset, $\mathbf{D}^{\mathrm{rec}}(f, x, y)$ is the reconstructed dataset, and $||.||_2$ represents the 2-norm of the matrix.

The reconstructed evaluation parameter above is for simulated data, in which $\mathbf{D}^{\mathrm{ori}}(f, x, y)$ is known. For the real data with unknown $\mathbf{D}^{\mathrm{ori}}(f, x, y)$, using information from observed data is more realistic. Thus, we modify the evaluation parameter in equation (9) to have equation (10) for field real data

$$E_{\mathrm{real}} = 20\log_{10}\left(\frac{\left\|\mathbf{D}^{\mathrm{obs}}(f,x,y)\right\|_2}{\left\|\mathbf{D}^{\mathrm{rec}}(f,x,y) - \mathbf{D}^{\mathrm{cal}}(f,x,y)\right\|_2}\right), \tag{10}$$

where $\mathbf{D}^{\mathrm{obs}}(f, x, y)$ denotes the observed data, $\mathbf{D}^{\mathrm{rec}}(f, x, y)$ denotes the reconstructed data with inserted observed data, and $\mathbf{D}^{\mathrm{cal}}(f, x, y)$ denotes the reconstructed data without observed data insertion.

Numerical examples

Synthetic data

Synthetic data without noise (41 × 41 traces) are shown in Figure 1a. The record length is 101 ms, the time sampling interval is 1 ms, the reflection coefficient of the horizontal and tilted linear event is 0.5 and -0.25, respectively, and the reflection coefficient of the shallow and deep bending event is 0.25 and 0.5, respectively. The wavelet unaffected by absorption and attenuation is stable during modeling travel time in this example. Figure 1b shows incomplete data with 30% randomly missing traces. We use Figure 1b to test the convergence speed and precision of the different threshold models. The maximum number of iterations is 50. We obtain the optimal inversely proportional model from the reconstructed evaluation parameter curve on the frequency slices at the 18th and 82nd samples.

Figures 2a and 3a show different threshold models for the frequency slices at the 18th and 82nd sample, respectively. In the legends of the two figures, Line denotes the linear model, Exp the exponential threshold,

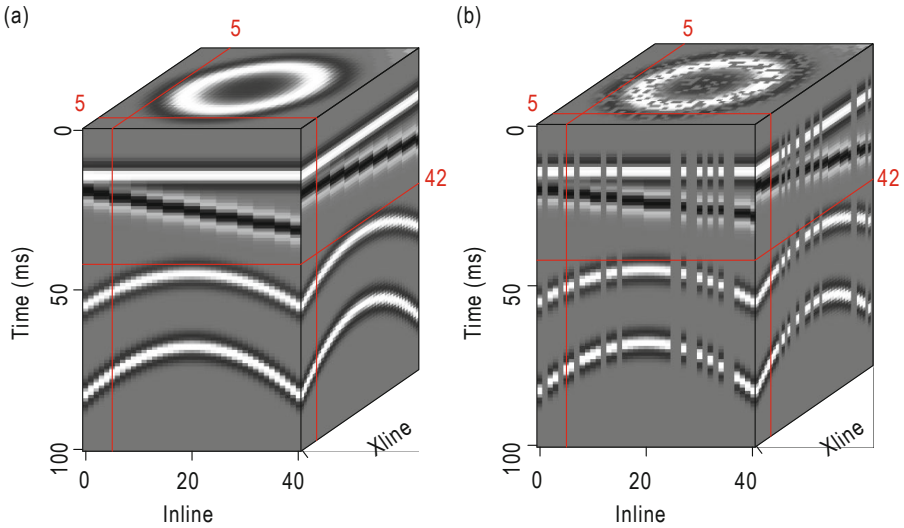

Fig.1 (a) Original data and (b) data with 30% of the traces missing.

Exp-0.5 the modified exponential threshold, Driven the data-driven model, Inv the inversely proportional model, and q = 0.5, 1.4, 2.2, and 3 are the different descent. Because the data-driven model describes the real spectrum energy distribution, we compare the data-driven model to the other models. From Figure 2a and 3a, we see that the linear model gradually decreases with increasing number of iterations. The descent rate of the exponential model is initially greater than that of the data-driven model and smaller in the small-coefficient section. Compared with the traditional exponential model, the descent rate of the modified exponential model increases initially and then decreases in the small-coefficient section. The descent rate of the inversely proportional model increases initially and decreases in the small-coefficient section with increasing q.

The threshold models in Figures 2a and 3a are used to interpolate the frequency slices. We can see from Figures 2b and 3b that the final reconstructed precision of the linear model is good and the convergence is the slowest. The convergence speed of the exponential model is faster and the final reconstructed precision is better than the data-driven model because the slow descent rate in the small-coefficient section is good for recovering weak events. Because the descent rate of the modified exponential model is initially greater and then smaller, the convergence speed and precision of the exponential model are both higher than the traditional exponential

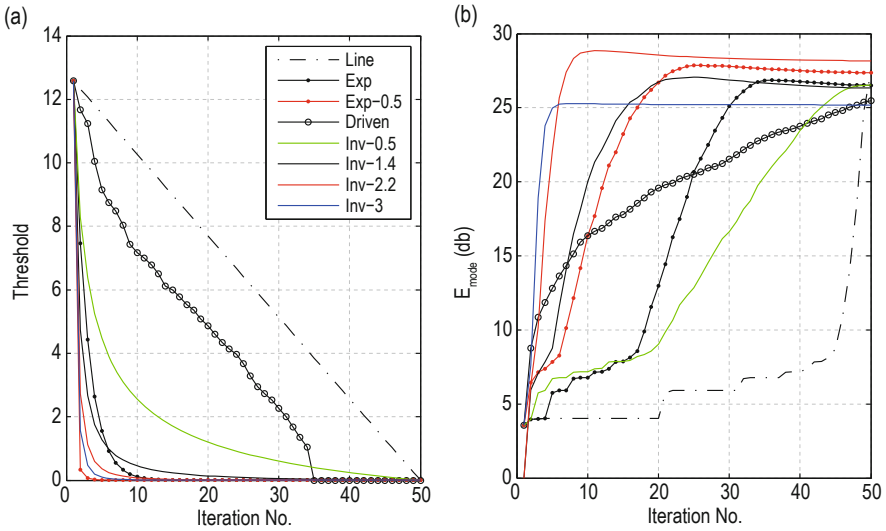

Fig.2 (a) Different threshold models for the frequency slice at the 18th sample and (b) E_{mode} curves of the different models.

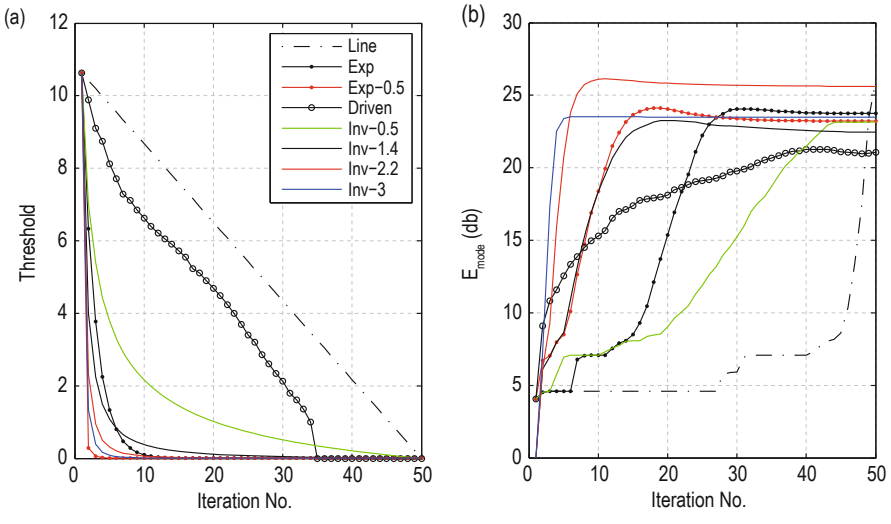

Fig.3 (a) Different threshold models for the frequency slice at the 82nd sample and (b) E_{mode} curves of the different models.

model. For q = 2.2, the inversely proportional model converges fast with the highest accuracy; thus, it can be used to reconstruct seismic data. For q = 3, the inversely proportional model has the fastest convergence; however, the evaluation parameter of the finally reconstructed data is low because of the loss of most of the effective Fourier coefficients. The advantage of the inversely proportional model for q = 2.2 is demonstrated by the reconstructed evaluation parameter curve for the 3D dataset in Figure 4.

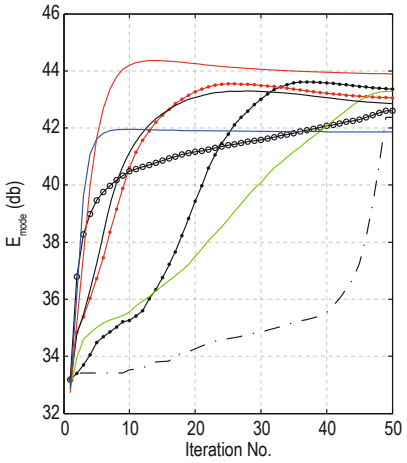

Fig.4 E_{mode} curves of the entire reconstructed 3D seismic dataset.

To analyze the denoising performance of descending Q for data-driven model in POCS reconstruction method, we create the incomplete dataset with noise in Figure 5a by adding random noise (SNR = 1.0 defined as the maximal amplitude of the signal to the maximal amplitude of the noise) to the data volume in Figure 1b. We perform the iterative reconstruction using the inversely proportional threshold model for q = 2.2. The maximum number of iterations is 50. We take the reconstructed data of the final iteration as output. The reconstructed data for Q = 0.2 and descending Q for the linear and data-driven models are respectively shown in Figures 5b, 5c and 5d. The quality of the reconstructed data for Q = 0.2 and descending Q for the linear model are almost the same, whereas the events in the reconstructed data for descending Q and the data-driven model are more continuous and with more high SNR. Note that the signal is slightly attenuated because the degree of noise attenuation using the descending Q and the data-driven model is based on the fact that the lower the SNR is, the higher the degree of noise attenuation is, that makes effective signal distorted.. To better show the advantage of descending Q and the data-driven model, we extract part of the incomplete seismic section in the inline direction CDP = 5 which also includes traces from 10 to 30 in the Xline direction, as shown in Figure 6. Incomplete data with noise are shown in Figure 6a. Figure 6b is the complete dataset without noise. The reconstructed data for Q = 0.2 and descending Q for the linear and data-driven models are separately shown in Figures 6c, 6d, and 6e. Figure 6e shows the noise attenuation for Q and data-driven model and is similar to the complete data without noise in Figure 6b. According to equation (9), the reconstructed evaluation parameter for Q = 0.2 and descending Q with linear and data-driven models in Figures 5b, 5c, and 5d is 22.08, 21.77, and 23.43, respectively. In addition, the reconstructed evaluation parameter for descending Q, and the exponential and inversely proportional model is 21.91 and 21.95, respectively. Clearly, the evaluation parameter is higher for descending Q with the data-driven model.

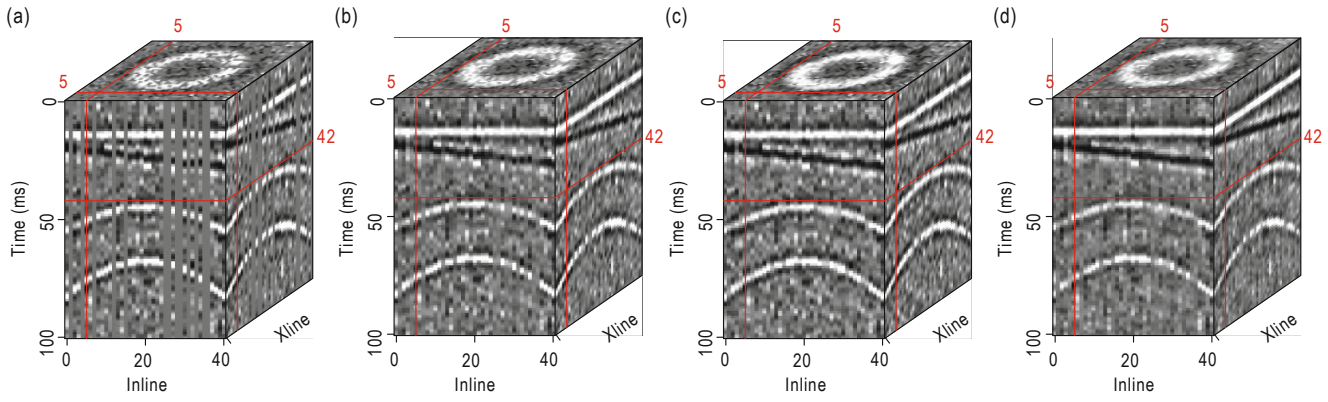

Fig.5 Reconstruction of a synthetic cube with 30% randomly missing traces for SNR = 1.0: (a) incomplete data, (b) reconstructed data for Q = 0.2, (c) reconstructed data for descending Q and the linear model, and (d) reconstructed data for descending Q and the data-driven model.

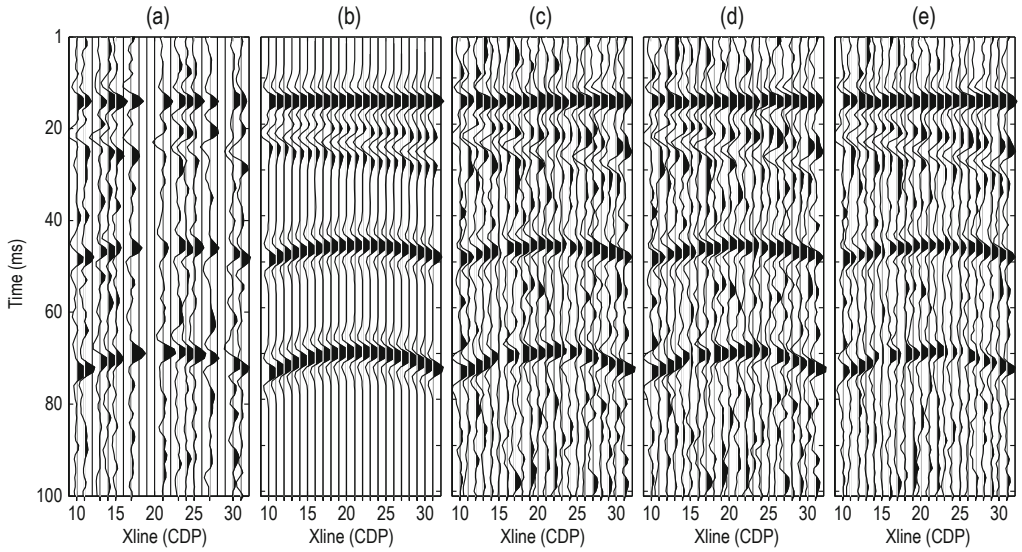

Fig.6 Original and reconstructed data for inline CDP = 5: (a) incomplete seismic data with noise, (b) complete seismic data without noise, (c) reconstructed data with Q = 0.2, (d) reconstructed data with Q based on the linear model, and (e) reconstructed data with Q based on the data-driven model.

Field data example

To further test the efficiency of our methods, the real data from a field of China are used for reconstruction. Figure 10 shows the observed data volume for inline slice 5 (side view), Xline slice 5 (front view), and time 50 ms (top view) and reconstructed data obtained by using different Q. Figure 10a shows part of the incomplete poststack 3D field data (missing 30% traces). The truncated record length is 301 ms and the sampling interval is 1 ms.

Before interpolating the entire 3D dataset, the optimal q is estimated from the reconstructed evaluation parameter of the frequency slices on typical strata. Because of absorption and attenuation, scattering and transmission at the reflection interface, and the complex structure create variability in the spectrum energy distribution in shallow, medium, and deep layers. Hence, we increase the number of frequency slices to be processed. If the optimal q of the different frequency slices varies, we perform Fourier-domain POCS reconstruction at different time windows. In this field example, owing to the short truncated record

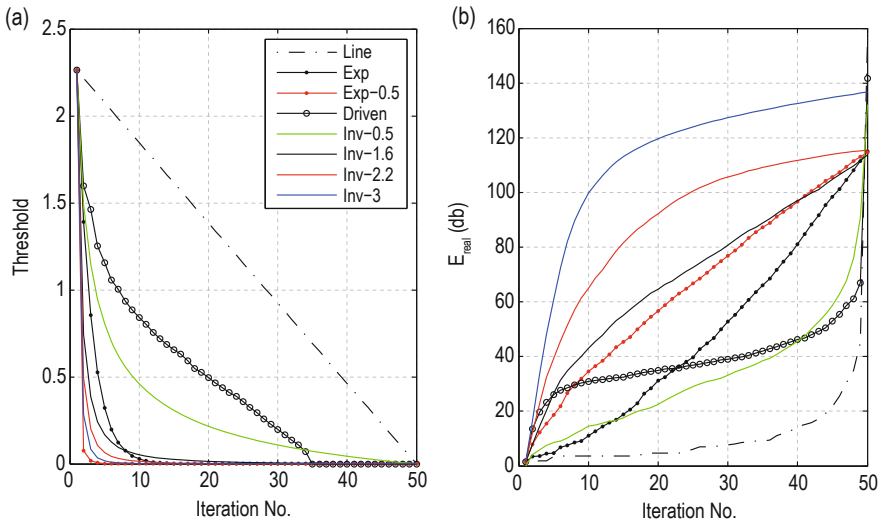

Fig.7 (a) Different threshold models for the frequency slice at the 50th sample and (b) E_{real} curves of the different models.

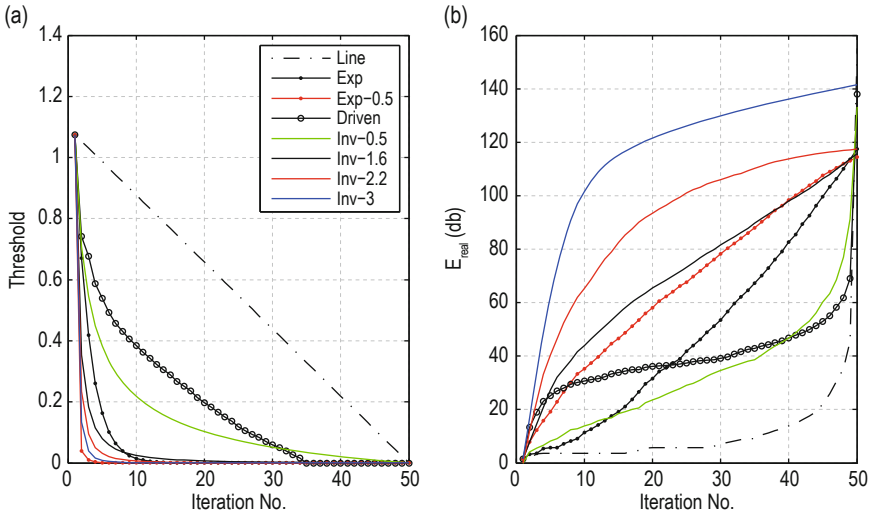

Fig.8 (a) Different threshold models for the frequency slice at the 190th sample and (b) E_{real} curves of the different models.

length and the simple structure, the absorption and attenuation are weak and the wavelet is stable. Thus, we only calculate the reconstructed evaluation parameter for two frequency slices to derive the optimal q. Figures 7a and 8b respectively show the threshold models on the frequency slices at the 50th and 190th samples.

The threshold models in Figures 7a and 8a are used in the data interpolation of the different frequency slices and the maximum number of iterations is 50. The reconstructed evaluation parameters in Figures 7b and 8b show that the inversely proportional model for q = 3 converges fast and with the highest accuracy, and can be used in the reconstruction of entire seismic dataset. The advantage of the inversely proportional model for q = 3 is shown by the reconstructed SNR curve of the entire 3D dataset in Figure 9.

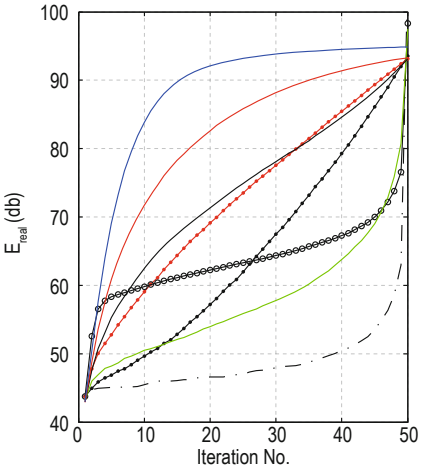

Fig.9 E_{real} curves of the entire 3D seismic dataset.

To test the advantage of descending Q for data-driven mode in real application, we perform the POCS reconstruction for data shown in Figure 10a using different reinserting weight strategies and the inversely

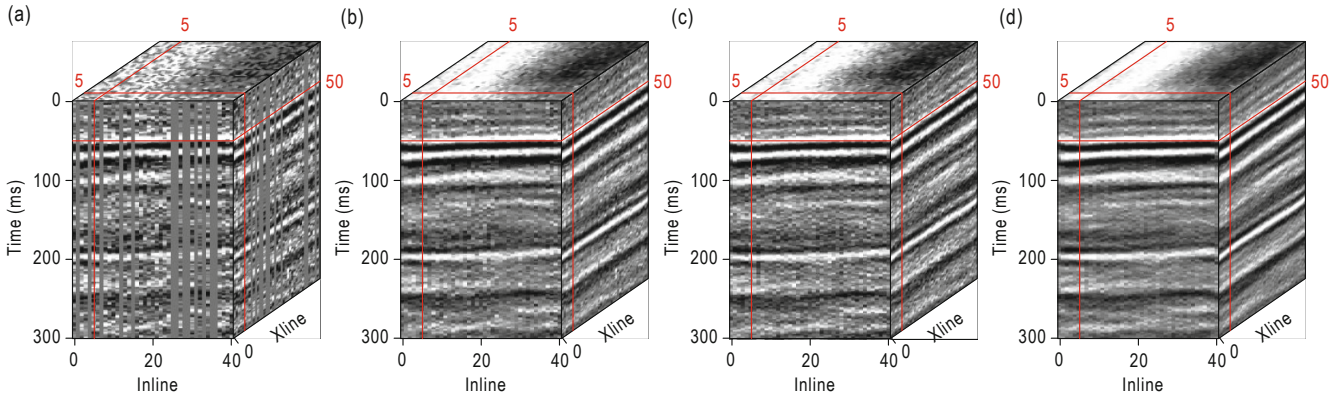

Fig.10 Reconstruction of the field cube: (a) irregularly missing data, (b) reconstructed data for Q = 0.2, (c) reconstructed data for Q and the linear model, and (d) reconstructed data for Q and the data-driven model.

proportional threshold model for q = 3. The maximum number of iterations is 50. We take the reconstructed data of the final iteration as output. The reconstructed data for Q = 0.2 and descending Q using the linear and data-driven models are shown in Figures 10b, 10c, and 10d, respectively. The reconstructed quality of the linearly descending weight is slightly superior to that of the constant weight. The noise attenuation in the reconstructed data for descending Q and the data-driven model is clearly visible and the weak events are reconstructed. To more clearly show the quality of the reconstructed data for different Q, we extract part of incomplete seismic section in the inline direction CDP = 5 that contains traces from 1 to 20 in the Xline direction and 1 to 250 ms in the time direction. Irregularly missing reconstructed data are shown in Figure 11a. The reconstructed data for Q = 0.2 and descending Q and the linear and data-driven models are shown in Figure 11b, 11c, and 11d, respectively. The comparison shows that noise is strongly attenuated in the reconstructed data for descending Q and the data-driven model.

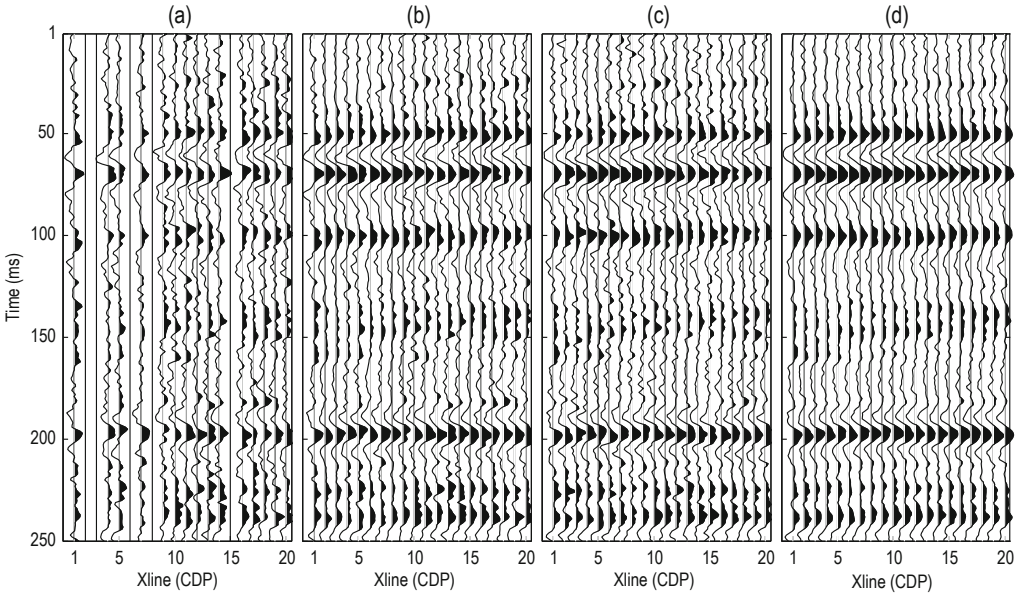

Fig.11 Original and reconstructed data for inline CDP = 5: (a) irregularly missing data, (b) reconstructed data for Q = 0.2, (c) reconstructed data for Q based on the linear model, and (d) reconstructed data for Q based on the data-driven model.

Conclusions

Convergence speed and precision are both needed for design of optimum threshold mode in POCS seismic reconstruction. To improve the flexibility of traditional threshold, we presented the inversely proportional threshold model and introduced dependent variable q to obtain different threshold curves of arbitrary descending rate. To improve the denoising performance of POCS reconstruction, we proposed a novel descending weight strategy according to data-driven mode. Firstly, we regularly sample for the distribution of spectrum energy according to the maximum iteration number, then in weight section, calculate weight value according to the percentage of each threshold in threshold section. Our method in this paper can be considered as the improvement of traditional denoising POCS reconstruction based on Fourier transform and can be generalized to other transform domains. The synthetic example and field application demonstrated the efficiency of improving computational efficiency, calculative precision and the SNR of the reconstructed data. The reinserting weight strategy has an instinctive shortage that a part of the original data and the reconstructed data are added to next iteration which makes the signal distorted when increases the SNR. Therefore, quality control is important for real application.

References

Abma, R., and Kabir, N., 2006, 3D interpolation of irregular data with a POCS algorithm: Geophysics, **71**(6), E91–E97.

Duijndam, A. W., Schonewille, M. A., and Hindriks, K., 1999, Reconstruction of band-limited signals irregularly sampled along one spatial direction: Geophysics, **64**(2), 524–538.

Galloway, E., and Sacchi, M. D., 2007, POCS method for seismic data reconstruction of irregularly sampled data: CSPG-CSEG-CWLS Joint Convention, 555.

Gao, J. J., Chen, X. H., Li, J. Y., et al, 2010, Irregular seismic data reconstruction based on exponential threshold model of POCS method: Applied Geophysics, **7**(3), 229–238.

Gao, J. J., Stanton, A., Naghizadeh, M., Sacchi, M. D., et al, 2013, Convergence improvement and noise attenuation consideration for beyond alias projection onto convex sets reconstruction: Geophysical Prospecting, **61**(suppl. 1), 138–151.

Gerchberg, R. W., and Saxton, W. O., 1972, A practical algorithm for the determination of phase from image and diffraction plane pictures: Optik, **35**(2), 227–246.

Hennenfent, G., and Herrmann, F., 2006, Seismic denoising with nonuniformly sampled curvelets: Computing in Science and Engineering, **8**(3), 16–25.

Kabir, M. M. N., and Verschuur, D. J., 1995, Restoration of missing offsets by parabolic Radon transform: Geophysical Prospecting, **43**(3), 347–368.

Kong, L. Y., Yu, S. W., Chen, L., et al., 2012, Application of compressive sensing to seismic data reconstruction: Acta Seismologica Sinica, **34**(5), 659–666.

Kreimer, N., and Sacchi, M. D., 2011, Evaluation of a new 5D seismic volume reconstruction method: Tensor completion versus Fourier reconstruction: Tensor Completion vs. Fourer, Reconstruction: CSPG-CSEG-CWLS Joint Convention, 1–5.

Li, H. F., and Du, M. H., 2003, Super-resolution Image Restoration Based on Improved POCS Algorithm: Journal of South China University of Technology (in Chinese), **31**(10), 24–27.

Liu, G. C., Chen, X. H., Guo, Z. F., et al., 2011, Missing seismic data rebuilding by interpolation based on curvelet transform: Oil Geophysical Prospecting (in Chinese), **46**(2), 237–246.

Malcolm, A. E., Hoop, M. V. D., and Rousseau, J. H. L., 2005, The applicability of dip moveout/azimuth moveout in the presence of caustics: Geophysics, **70**(1), S1–S17.

Menke, W., 1991, Applications of the POCS inversion method to interpolating topography and other geophysical fields: Geophysical Research Letters, **18**(3), 435–438.

Naghizadeh, M., and Sacchi, M. D., 2010, Beyond alias hierarchical scale curvelet interpolation of regularly and irregularly sampled seismic data: Geophysics, **75**(6), WB189–WB202.

Naghizadeh, M., and Sacchi, M. D., 2009, f-x adaptive seismic-trace interpolation: Geophysics, **74**(1), V 9–V16.

Oropeza, V., and Sacchi, M., 2011, Simultaneous seismic data denoising and reconstruction via multichannel singular spectrum analysis: Geophysics, **76**(3), V25–V32.

Papoulis, A., 1975, A new algorithm in spectral analysis and band limited extrapolation: IEEE Transactions on Circuits and Systems, **CAS–22**(9), 735–742.

Ronen, J., 1987, Wave-equation trace interpolation: Geophysics, **52**(7), 973–984.

Spitz, S., 1991, Seismic trace interpolation in the F-X domain: Geophysics, **56**(6), 785–794.

Trad, D. O., 2009, Five-dimensional interpolation: Recovering from acquisition constraints: Geophysics, **74**(6), V123–V132.

Trad, D. O., Ulrych, T. J., and Sacchi, M. D., 2002, Accurate interpolation with high-resolution time-variant Radon transform: Geophysics, **67**(2), 644–656.

Trickett, S., Burroughs, L., Milton, A., et al, 2010, Rank-reduction-based trace interpolation: 80th Ann. Internat. Mtg., Soc. Explor. Geophys., Expanded Abstracts, 1989–1992.

Wang, S., Gao, X., and Yao, Z., 2010, Accelerating POCS interpolation of 3D irregular seismic data with graphics processing units: Computers and Geosciences, **36**(10), 1292–1300.

Wang, S. Q., and Zhang, J. H., 2014, Fast imaging in painting using exponential-threshold POCS plus conjugate gradient: The Imaging Science Journal, **62**(3), 161–170.

Zhang, H., and Chen, X. H., 2013, seismic data reconstruction based on jittered sampling and curvelet transform. Chinese Journal of Geophysics (in Chinese), **56**(6), 1637–1649.

Ge Zi-Jian received his B.S. (2011) in Exploration Technology and Engineering and M.S. (2014) in Earth Exploration and Information Technology from Southwest Petroleum University. He is presently a Ph.D. candidate in China University of Petroleum (Beijing), majoring in Geological Resources and Geological Engineering. His research interests are seismic data processing and reservoir characterization.